Heterogeneous Soot Nanostructure in Atmospheric and Combustion Source Aerosols

Michael D. Hays*,† and Randy L. Vander Wal‡

United States Environmental Protection Agency, National Risk Management Research Laboratory, Research Triangle Park, North Carolina 27711, and The Universities Space Research Association (USRA) at The NASA−Glenn Research Center

In this work, high-resolution transmission electron microscopy images of microscopic soot emissions from wildfire and from a wide range of anthropogenic combustion sources (e.g., electrical utility and institutional oil boilers, jet aircraft, and heavy-duty diesel trucks) are presented. The soot nanostructures of individual particles in these emissions are predominantly heterogeneous, decidedly influenced by the fuel composition and by the particular combustion process the fuels undergo, and reveal the mechanisms underlying primary soot particle inception and growth. A lattice fringe analysis shows that differences among the soot nanostructures are measurable. To study whether these differences might identify the combustion source types contributing to ambient aerosols, we also examine the nanostructures of individual atmospheric particles collected at two spatially diverse United States locations (Duke Forest, North Carolina, and the Northern Front Range, Colorado). We find that the elemental carbon structure in airborne particles is mixed internally and externally and does, in fact, reflect contributions from different anthropogenic and biomass burning sources. An improved understanding of the soot nanoheterogeneity in airborne and combustion particles is likely to greatly influence $PM_{2.5}$-related health and source apportionment research.

Introduction

Global emissions estimates of submicrometer soot particles [also referred to as elemental or black carbon (EC or BC); hereafter referred to as EC or soot] are as high as 12−17 Tg/year.[1] Formed from the incomplete combustion of biomass and fossil fuels, soot particle emissions from anthropogenic and wildfire sources have received ever-increasing attention, owing to their direct and indirect[2] roles in climate forcing and the potential health risks they pose.[3]

The chemical reactivity and physical and radiative properties of soot are dependent on its nanostructure,[4] a term referring to the degree of atomic order as manifested by graphitic layer plane segments and their physical relation to each other. The details of soot structure at the nanolevel are normally gleaned from images recorded using a high-resolution transmission electron microscope (HR-TEM), a high-magnification instrument with spatial resolution better than 0.2 nm. Sample examinations by HR-TEM can furnish information on atom arrangements, surface topography and texture, particle morphology, material crystallinity, and composition. Extensive information on the mixing state and chemical heterogeneity of aerosols is also obtainable with HR-TEM.

In laboratory studies using a high-temperature furnace, the combustion of different fuels has produced considerably different soot nanostructures.[5] These differences in soot nanostructure were shown to be mainly dependent upon the fuel composition, the combustion process, and the combustion temperature.[6,7] When a form of computational image analysis, lattice fringe analysis, is used, soot nanostructure and its variations could also be quantified. In essence, quantification included parametrizing length, curvature, and separation distance between the carbon lamella. Substantial differences in these categories have translated into colloquial characterization of the carbon as graphitic, fullerenic, or amorphous. The question to be addressed here is whether similar differences might be manifested in the soot produced from biomass burning (e.g., wood stoves or wildfire) and in commonly used fossil fuel combustion devices (e.g., utility boilers, vehicles, etc.) given the wide variation in fuels and combustion conditions. If plausible, these differences could be used to help identify or fingerprint the combustion sources contributing to ambient aerosols or could be used to partly explain the causal mechanisms for the adverse health effects of aerosols. Such research activity could support source apportionment and health studies with potentially significant regulatory implications.

Indeed, HR-TEM studies have begun to indicate qualitative differences in nano- and microstructure and morphology among carbonaceous particles from anthropogenic and wildfire sources

* To whom correspondence should be addressed. E-mail: hays.michael@epa.gov.
† United States Environmental Protection Agency.
‡ USRA.

(1) International Panel on Climate Change. *Climate Change 2001: The Scientific Basis*; Cambridge University Press: New York, 2001.
(2) Hansen, J.; Nazarenko, L. *Proc. Natl. Acad. Sci. U.S.A.* **2004**, *101*, 423−428.
(3) Donaldson, K.; Tran, L.; Jimenez, L. A.; Rodger, D.; Newby, D. E.; Mills, N.; William, M.; Stone, V. *Part. Fibre Toxicol.* **2005**, *2*, DOI: 10.1186/1743-8977-1182-1110.
(4) van Poppel, L. H.; Friedrich, H.; Spinsby, J.; Chung, S. H.; Seinfeld, J. H.; Buseck, P. R. *Geophys. Res. Lett.* **2005**, *32*, DOI: 10.1029/2005GL024461.
(5) Wornat, M. J.; Hurt, R. H.; Yang, N. Y. C.; Headley, T. J. *Combust. Flame* **1995**, *100*, 131−143.
(6) Vander Wal, R. L.; Tomasek, A. J. *Combust. Flame* **2003**, *136*, 129−140.
(7) Vander Wal, R. L.; Tomasek, A. J. *Combust. Flame* **2003**, *134*, 1−9.

(for example, see and compare the TEM images in refs 8−10). However, visual evidence within the HR-TEM images alone has not always adequately revealed the subtle variations among the complex networks of lamella borne from the different fossil fuel combustion sources (as evidenced by panels c and d in Figure 1 of ref 8).[8] Assuming soot nanostructure is to support sound decision making in source apportionment and other health-related PM$_{2.5}$ research activities (PM$_{2.5}$ refers to particulate matter that is 2.5 μm or smaller in size), a quantitative analysis and understanding of the soot nanostructure from a range of combustion sources will be needed. Yet, we know of only one study providing such quantitative data, and its focus concerns primarily diesel soot emissions.[11]

In this work, we assemble HR-TEM images of soot from a range of anthropogenic and pyrogenic emissions sources, which contribute significantly to the atmospheric aerosol burden. The soot nanostructures over select particle areas are quantified using lattice fringe analysis. The quantitative results illuminate the clear visual distinction between biomass burning and fossil fuel combustion soots. And although there are visual differences in nanostructure among the fossil fuel combustion soots examined (corroborating our initial laboratory studies), the fact that these differences were less evident generally applies. Visual inspection of nanostructure did grant us the ability to reveal the mechanisms underlying primary soot particle inception and growth and the combustion and fuel source characteristics. It also reveals internally variable elemental carbon structure and composition within individual primary soot particles from the same fossil fuel combustion source.

To finish, we show that the nanostructures of individual atmospheric particles collected at spatially diverse U.S. locations (Duke Forest, North Carolina, and the Northern Front Range, Colorado) are largely internally and externally mixed EC assemblages, which reflect specific fuel and combustion source contributions. These data draw a direct link between atmospheric soot and primary combustion source emissions. The value of developing an approach that uses the relatively nonreactive EC component of PM for apportionment is considerable, especially in light of the recent evidence showing that the condensable organic markers commonly used in linear factor analysis and chemical mass balance models are being photochemically oxidized in aged, regionally transported summertime aerosols.[12]

General Picture of Soot Formation. Fuel pyrolysis occurring at relatively low combustion temperatures generates the molecular species, energy, and conditions necessary for mass growth of soot nuclei.[13] Generally, molecular species grow as polycyclic aromatic hydrocarbons (PAH) of ever increasing molecular weight.[14] Ultimately, the supersaturation of very high mass species causes initial condensation, which may be aided by reactive processes.[15] Subsequent carbonization followed by continued molecular mass addition to the growing particle leads to primary soot particles.[16] Depending upon the nascent fuel composition and combustion temperature, different species such as PAH or acetylene can contribute to soot mass growth.[17] During the growth process, agglomeration occurs, resulting in the fractal aggregates typical of soot particles. Traditionally, most analysis of soot has pertained to the microstructure or overall (micrometer) size of the aggregate.[18] The primary motivation for this emphasis stems from the inhalation concerns associated with aerosols, soot in particular, which has led to the Environmental Protection Agency PM$_{2.5}$ criteria. Submicrometer aerosol particles can penetrate deep into the lung, thereby presenting a significant health hazard.[19]

Fractal geometry is the common size method used to describe aggregate structure, and such a description finds use in modeling aerosol dynamics and the absorption and scattering properties of soot.[20] However, most such analyses are conducted on laboratory soot, and only recently has the fractal methodology been applied to PM produced by diesel engines.[21] By comparison, soot nanostructure is recognized as being (i) of greater importance to understanding soot reactivity and (ii) more reflective of the soot formation conditions and of the gas-phase species contributing to soot formation. We would add that the nature of soot organization is likely to affect biochemical-mediated particle uptake in lung epithelial and macrophage cell lines. Full comprehension of different soot nanostructures may therefore also be justified when developing an understanding of source-related PM$_{2.5}$ health mechanisms.

Surface processes ultimately influence the soot nanostructure by mediating the addition of gas-phase hydrocarbons to the particle. Different gas-phase molecular species will likely diffuse to the surface at different rates and may yield different surface structures with consequences for subsequent carbon layer plane growth and assembly. The surface reaction, growth, and assembly processes are considered to be fully dependent on these gas-phase molecular species; therefore, the final soot particle nanostructure is expected to reflect the gas-phase flame chemistry and is interpreted with the surface-mediated processes implicit.[22]

Experimental Section

Sample Matter. In all, seven aerosol samples were analyzed for soot nanostructure by HR-TEM, five from source emissions testing and two from sampling the atmosphere. The emissions samples selected for analysis were within the oil fuel combustion (industrial, commercial, residential, and electrical utilities; 46.3 Gg/year), transportation (230 Gg/year from highway and off-highway diesel and aircraft), and biomass burning (wildfires, agricultural

(8) Chen, Y.; Shah, N.; Huggins, F. E.; Huffman, G. P. *Environ. Sci. Technol.* **2005**, *39*, 1144−1151.

(9) Chen, Y.; Shah, N.; Huggins, F. E.; Huffman, G. P. *Atmos. Environ.* **2006**, *40*, 651−663.

(10) Posfai, M.; Gelencser, A.; Simonics, R.; Arato, K.; Li, J.; Hobbs, P. V.; Buseck, P. R. *J. Geophys. Res.* **2004**, *109*, DOI: 10.1029/2003JD004169.

(11) Palotas, A., B.; Rainey, L. C.; Feldermann, C. J.; Sarofim, A. F.; Vander Sande, J. B. *Microsc. Res. Tech.* **1996**, *33*, 266−278.

(12) Robinson, A. L.; Donahue, N. M.; Rogge, W. F. *J. Geophys. Res.* **2006**, *111*, DOI: 10.1029/2005JD006265.

(13) Frenklach, M.; Wang, H. Detailed Modeling of Soot Particle Nucleation and Growth. The Twenty-Third (International) Symposium on Combustion, Orleans, France, 1990; The Combustion Institute: Pittsburgh, PA, 1990; pp 1559−1566.

(14) Grieco, W. J.; Howard, J. B.; Rainey, L. C.; Vander Sande, J. B. *Carbon* **2000**, *38*, 597−614.

(15) Miller, J. H. The Kinetics of Polynuclear Aromatic Hydrocarbon Agglomeration in Flames. The Twenty-Third (International) Symposium on Combustion, Orleans, France, 1990; The Combustion Institute: Pittsburgh, PA, 1990; pp 91−98.

(16) Vander Wal, R. L. *Combust. Flame* **1998**, *112*, 607.

(17) McKinnon, J. T.; Howard, J. B. The Roles of PAH and Acetylene in Soot Nucleation and Growth. The Twenty-Fourth Symposium (International) on Combustion, Sydney, Australia, 1992; The Combustion Institute: Pittsburgh, PA, 1992; pp 965−971.

(18) Manzello, S. L.; Choi, M. Y. *Int. J. Heat Mass Transfer* **2002**, *45*, 1109−1116.

(19) Tsuda, A.; Rogers, R. A.; Hydon, P. E.; Butler, J. P. *Proc. Natl. Acad. Sci. U.S.A.* **2002**, *99*, 10173−10178.

(20) Koylu, U. O.; Faeth, G. M. *J. Heat Transfer* **1993**, *115*, 409−417.

(21) Lee, K. O.; Zhu, J. *Evolution in Size and Morphology of Diesel Particulates along the Exhaust System*; SAE Paper 2004-01-1981; Society of Automotive Engineers: Warrendale, PA.

(22) Frenklach, M.; Ping, J. *Carbon* **2004**, *42*, 1209−1212.

fires, prescribed burning, and residential wood combustion, 1.3 Tg/year) source sectors. These sources were selected using their impact on air quality as a basis; combined, they accounted for approximately 25% of all anthropogenic fine aerosol emissions (6.2 Tg/year) in the U.S. in 2002.[23] Global estimates of EC emissions from these sources range from 5.6 to 11.0 Tg/year,[24] accounting for approximately 50% of the world's yearly EC emissions. We use EC as a surrogate for soot and its nanostructure throughout. However, because EC is "operationally" defined and subject to artifacts, it may incorrectly predict the mass attributable to a specific soot nanostructure imaged by HR-TEM. To the best of our knowledge, these are the first direct TEM observations of jet engine and plant- and institutional-scale oil boiler soot nanostructures.

Except where otherwise indicated, aerosol was collected using a dilution sampling system (DSS) reported previously.[25] The dilution factor varied, depending upon the system and test. Teflon and high-volume quartz filter media served to capture the filterable $PM_{2.5}$. These were subsequently processed for HR-TEM analysis as indicated. The sample age spanned from ~1 to 9 years. During this time, the samples were stored in an ultralow-temperature freezer at a maximum temperature of -45 °C. An effect on nanostructure due to either the wide time gap between sample collection and analysis or to the storage conditions was not expected. A detailed description of each source and sample follows.

Plant-Scale Electrical Utility Boiler (432 GJ) Firing Residual Oil. Aerosol emissions from a front-fired fossil fuel steam generator burning No. 6 residual fuel oil were sampled using the DSS. This aerosol contained less than 1% w/w carbon. Results of a No. 6 residual fuel analysis found the following: C, 87.85; H, 7.34; O, 1.87; N, 0.57; S, 2.35; ash, 0.02—all values are given as percentages. Chlorine content in No. 6 residual fuel oil can be as much as 500 ppm.

Institutional-Scale Boiler (67 GJ) Firing Distillate Oil. This $PM_{2.5}$ emissions sample was collected from an institutional-scale water tube boiler firing No. 2 distillate oil ($\rho = 0.84$ g/L). Upon visual inspection, the collected aerosol appeared black. Thermal-optical analyses confirmed that up to 34% w/w of the carbon was elemental carbon or soot. Results of a No. 2 distillate fuel analysis found the following: C, 85.93; H, 13.66; O, 0.26; N, 0.03; S, 0.09; Cl, ~300 ppm; ash, 0.01—all values are given as percentages.

Jet Aircraft Engine Exhaust. A fine aerosol sample was collected from the emissions of a commercial (General Electric CFM-56-2-C1) turbofan engine mounted on a Boeing DC-8 jet aircraft. Tests were conducted as part of the NASA Air Particulate Emissions Experiments program. The sample integrated engine operating tests were conducted at four power (thrust) settings—7% (idle), 30% (approach), 85% (climb-out), and 100% (take-off)—typical of the landing and take-off cycle at commercial airports. This PM sample comprised nearly 35% w/w EC. Jet propulsion fuel No. 8 (JP-8; $\rho_{15\ °C} = 0.8199$ g/cm³; heat of combustion = 43.2 MJ/kg) was the base fuel. Compositional analyses of this jet fuel showed the following: S, 409 ppm; H, 13.7% w/w; aromatics, 17.9% v/v.

Highway, Heavy-Duty Diesel Truck Emissions. The diesel soot sample was collected as an on-road aerosol emission from a high-mileage, 1990 Kenworth long-haul, heavy-duty truck with a series 60 Detroit diesel engine. Sample exhaust was diluted (1:56) with compressed, dry, HEPA-filtered air directed to a series of three eductors (1:20 dilution each). A $PM_{2.5}$ cyclone was positioned in the dilution system upstream of the sample filter. Fine particulate matter in the diesel truck exhaust was sampled on a Teflon filter. That filter sample was visibly black and contained 70% EC on a mass basis.

Ponderosa Pine (*Pinus* sp.) Forest Wildfire. Fresh green needles, small branches, twigs, and cones were gathered in a western

U.S. Ponderosa pine forest and burned in a test enclosure as they are burned in the field. Milligrams of aerosol emissions from this simulated wildfire were sampled. The collection, handling, and burning of the biomass fuel were described by Hays et al.[26] An analysis of fuel composition found the following: C, 44.6; H, 5.4; N, 0.7; O, 31.1; S, 0.1—all values are given as percentages. Though this aerosol was virtually all carbon, it comprised less than 2% w/w EC matter.

Ambient $PM_{2.5}$ Collected in Duke Forest. The Duke Forest ambient sample is a 2-day composite sample collected from Friday July 25, 2003 at 6:45 PM until Sunday, July 27 8:05 PM using an MSP high-volume sampler, sampling through a $PM_{2.5}$ head at 270 lpm at Chapel Hill, NC. No denuders were used. The organic carbon (OC)/EC ratio was 11:1, which was typical of about half of the samples collected at this time and a bit higher than others. The sample is expected to comprise 90% carbon from the oxidation of terpenic hydrocarbons, which likely polymerized into larger molecules as some studies have suggested.[27] The EC is probably from diesel and biomass burning sources, although potassium data and meteorology do not support a significant fire contribution. The Duke Forest site is located near a local access road, thus, is expected to capture a small fraction of vehicle soot. On a wider spatial scale, this field-monitoring site is located in a 32 km² forest surrounded by a thickly settled urban area.

Northern Front Range Air Quality Study. The second ambient $PM_{2.5}$ sample is a 24-h sample (12/20/1996−12/21/1996), collected as part of the Northern Front Range Air Quality Study at the Welby site in the northeast Denver area. Aerosol was collected on a 79 mm Gelman Zefluor filter with an MSP high-volume virtual impactor operating at a 0.28 m³/min flow rate; the sampler had a 2.5 μm aerodynamic cut point. On December 20, 1996 at the Welby site, the OC/EC ratio was nearly 1:1 at a total carbon concentration of ~10 μg/m³. Receptor modeling attributed the majority of EC to light-duty gasoline (cold starts) and diesel vehicles. A coal-fired power plant and petroleum refinery were the major industrial facilities operating regionally.[28]

Sample Preparation. The process for creating the TEM sample consisted of removing a portion of the collected soot from the sample filter and dispersing it upon a TEM grid. A portion of the sample filter was removed by cutting. This piece typically measured 1 cm² in area. Within a new glass sample bottle, the filter section and 5 mL of 200-proof ethanol were agitated by sonication. Material was readily released from the filter and observed as a clouding of the solution. Though a period of 1 min typically resulted in a high degree of removal of material from the filter, as judged qualitatively by its change in opacity, typically a sonication time of 10 min was used to ensure near total removal. A drop of the dispersed solution was then placed upon the lacey TEM grid. By drying through evaporation, suspended material was deposited upon the TEM grid. All of the collected soots were examined using this approach.

The elemental carbon composition of soot was the main focus of our study. Prior analyses confirmed each soot examined here as comprising some fraction of elemental carbon. In such carbonaceous soots, inclusions and other heterogeneous material are not readily extracted (e.g., fullerenes imbedded within flame soot are generally not extractable). Redeposition of soluble organic matter, if present, following drying of the ethanol−soot droplet is readily observed as a thin film on the particles and grid. This can greatly obscure imaging at high magnifications. Subsequent sample preparation employed a dry transfer process for transferring soot from selected collection filters to TEM grids. For two organic soots—namely, the wildfire and aircraft soots—treated this way, changes in morphology or nanostructure were not observed, suggesting an

(23) U.S. EPA, Office of Air Quality Planning and Standards−Clearinghouse for Emission Inventories and Emission Factors. http://www.epa.gov (accessed May 2005).

(24) Bond, T. C.; Streets, D. G.; Yarber, K. F.; Nelson, S. M.; Woo, J.-H.; Klimont, Z. *J. Geophys. Res.* **2004**, *109*, D14203.

(25) Hildemann, L. M.; Cass, G. R.; Markowski, G. R. *Aerosol Sci. Technol.* **1989**, *10*, 193.

(26) Hays, M. D.; Geron, C. D.; Linna, K. J.; Smith, N. D.; Schauer, J. J. *Environ. Sci. Technol.* **2002**, *36*, 2281−2295.

(27) Claeys, M.; Graham, B.; Vas, G.; Wang, W.; Vermeylen, R.; Pashynska, V.; Cafmeyer, J.; Guyon, P.; Andeae, M. O.; Artaxo, P. E.; Maenhaut, W. *Science* **2004**, *303*, 1173−1176.

(28) Watson, J. G.; Fujita, E. M.; Chow, J. C.; Zielinska, B.; Richards, L. W.; Neff, W.; Dietrich, D.; Northern Front Range Air Quality Study: Final Report. Desert Research Institute: Reno, NV, 1998.
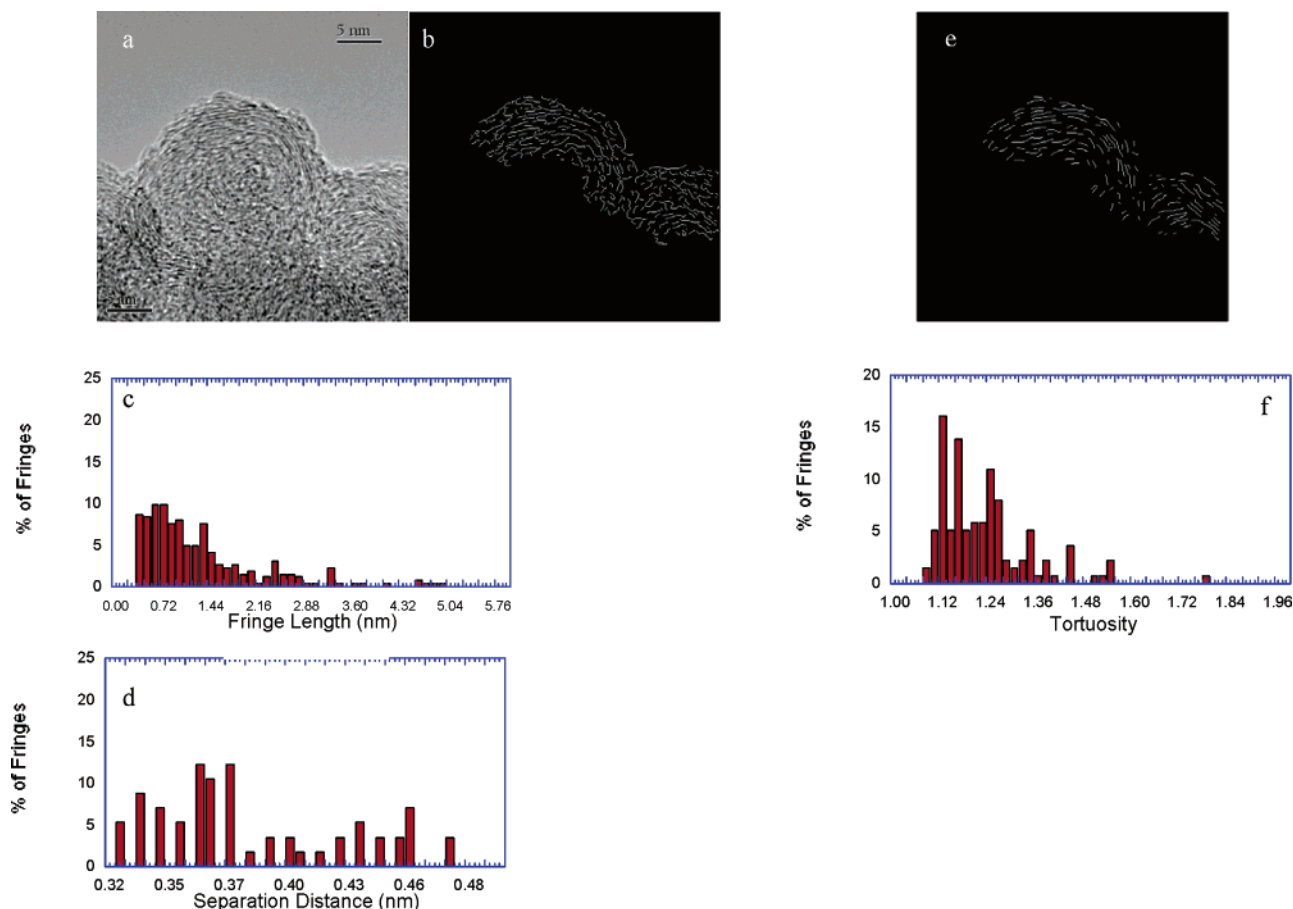
Figure 1. Shown are the bright-field HR-TEM image (a), the corresponding skeleton image (b), derived histograms of fringe length (c) and separation distance (d), the image skeleton for calculation of tortuosity (e), and histogram of fringe tortuosity (f) for the soot derived from the plant-scale electrical utility boiler firing residual oil.

absence of chemical or physical solvent effects due to the solvent-based TEM sample preparation.

High-Resolution Transmission Electron Microscopy (HR-TEM). HR-TEM images were taken using a Phillips CM200 with a Gatan image filter for digital imaging with live Fourier transforms with a nominal resolution of 0.14 nm. The instrument operated at 200 keV using LaB6 filament. Typically, three or more locations, well-separated on the TEM grid, were examined to verify uniformity of the sample, specifically the soot morphology and primary particle (nano)structure. These locations were examined at a series of progressive magnifications to determine the consistency of the particular nanostructure. If variability was observed, additional locations were analyzed to resolve the predominant form. Images were collected digitally from portions of the sample that were best imaged (isolated regions of soot aggregates where primary particles were not overlapped by other primary particles along the electron beam axis).

HR-TEM Lattice Fringe Image Analysis. Though the HR-TEM images are helpful in revealing the nanostructure of soots, they only provide a qualitative measure. A more quantitative measure may be obtained by a lattice fringe analysis of the HR-TEM images,[29] so called because the carbon lamella appear as "fringes" under HR-TEM imaging. With the advent of digital imaging and computer-based image processing, we have developed image processing algorithms expressly for this purpose. Previous papers have detailed the processing of images and demonstrated validation against the traditional measures of Raman and X-ray diffraction for the graphitic structure in a series of heat-treated carbons and as a nanoscale metrology tool.[30]

(29) Shim, H.-S.; Hurt, R. H.; Yang, N. Y. C. *Carbon* **2000**, *38*, 29−45.
(30) Vander Wal, R. L.; Tomasek, A. J.; Street, K. W.; Hull, D. R.; Thompson, W. K. *Appl. Spectrosc.* **2004**, *58*, 230−237.

Results and Discussion

HR-TEM and Lattice Fringe Analyses of Source Soots. Generally, lower-magnification TEM images of particle soot from the selected sources revealed aggregate morphology with fairly significant merging of primary particles (data not shown). The degree of aggregate compactness and particle merging varied by combustion source; for example, the wildfire particles were fully merged compared with those from fossil-fuel combustion. Within the fossil-fuel combustion category, the primary particles from the institutional-scale oil boiler were fused to the greatest extent. Even though the primary particles observed were not clearly defined typically, we estimated their size ranging from approximately 20 to 100 nm and varying within and across source types. They appeared mostly as spheroids with distortions and irregularities being revealed upon close inspection. In contrast to laboratory-generated soots exhibiting an often-cited structure consisting of point-contacting spheres assembled into branched fractal aggregates, the aggregates observed here were rather compact, generally lacking such "traditional" structure. Therein, aerodynamic size parameters for many of the primary and aggregate particles observed are less meaningful. Despite this lack of macrostructure, a bimodal size distribution composed of particles either much smaller or larger than the reported aggregate or primary particle (as might be expected in either a nucleation or agglomeration mode) was not seen.

Figures 1−5 each include high-magnification TEM images (resolving individual carbon lamella) of soots from globally relevant anthropogenic emissions sources along with their
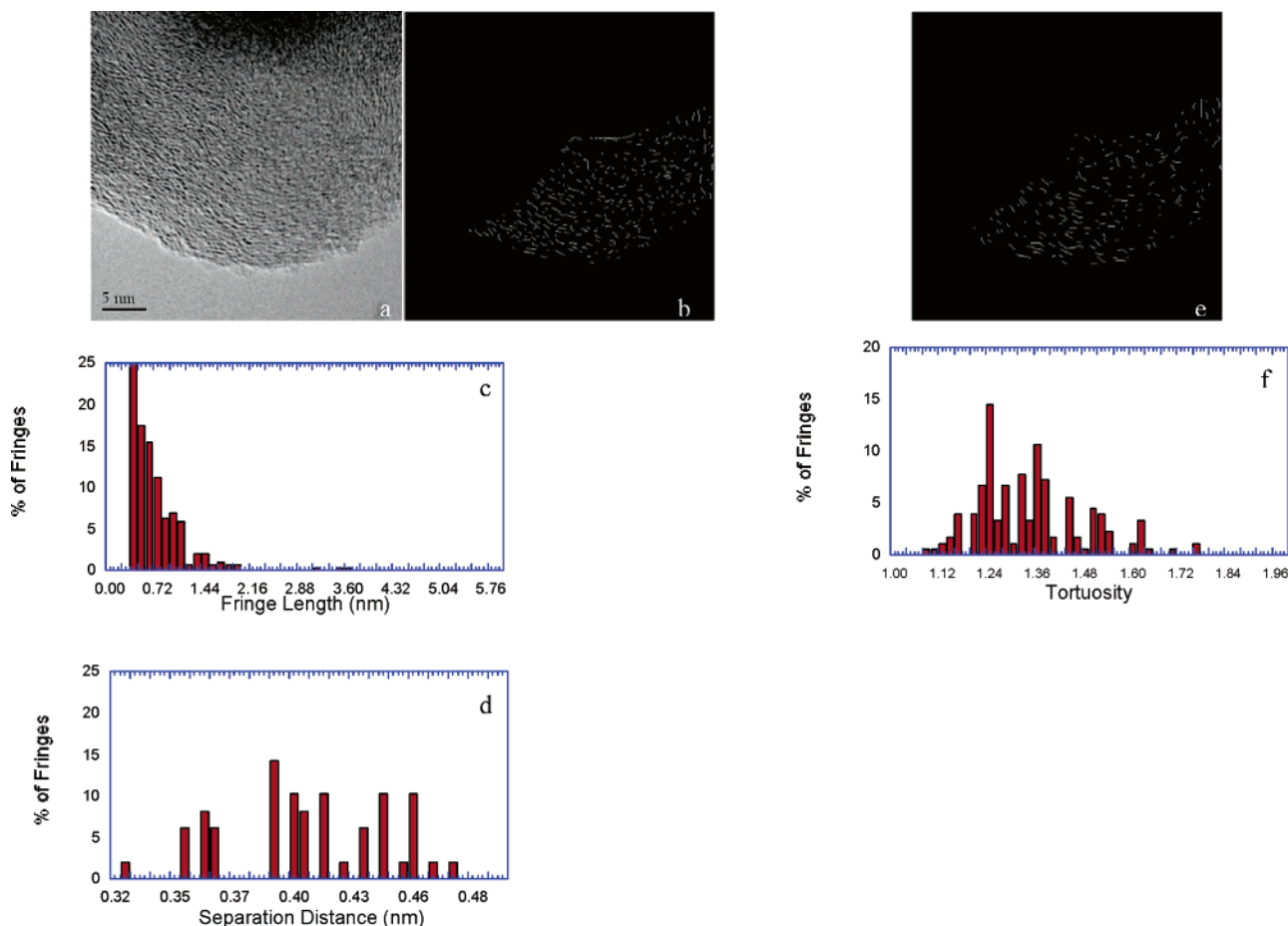
Figure 2. Shown are the bright-field HR-TEM image (a), the corresponding skeleton image (b), derived histograms of fringe length (c) and separation distance (d), the image skeleton for calculation of tortuosity (e), and histogram of fringe tortuosity (f) for the soot derived from the institutional-scale boiler fueled with distillate oil.

corresponding fringe analysis plots. In the next sections, observations of each source's nanostructure with respect to particle nucleation and growth, combustion conditions, and fuel chemistry are considered.

Plant- and Institutional-Scale Oil Boilers. When tested, the plant-scale electrical utility boiler (432 GJ) firing residual oil was operating at roughly half of its permitted load with a five-field electrostatic precipitator as the only control device. These test conditions resulted in a $PM_{2.5}$ mass emission factor of 2.2 g/kg of fuel burned (averaged over 22 h of sampling). Sulfur was the single most predominant element. The fine aerosol collected was sulfur-enriched (∼60% w/w; determined by X-ray fluorescence) in the accumulation mode specifically between the diameters of 400−650 nm. As mentioned, the PM emissions from this boiler comprised less than 1% w/w carbon; the EC/OC ratio was as much as 2:1. The especially diminutive organic carbon concentration made it impractical to apply any conventional, off-line analytical methodology to determine the identity or level of organic markers in this filter sample. These are the compounds normally utilized for source attribution and apportionment. The carbon contribution estimate of this source may therefore be erroneously neglected when using only organic markers to apportion airborne PM. We justify focusing on the soot component in these emissions using HR-TEM on the basis of (i) its single-particle sensitivity, (ii) the larger fraction of EC (as opposed to OC) in this particular sample, and (iii) the significant global EC emissions from oil combustion for electrical power generation (approximated at 13 Gg/year).[31]

The HR-TEM bright-field image of soot from the plant-scale boiler emissions is shown in Figure 1. The nanostructure possesses a radial variation. Along the particle perimeter, the lamella are distinct while the interior is comprised of short, disorganized segments; this is somewhat analogous to our observation of diesel soot−given later. Such differences in nanostructure may reflect a combination of different combustion temperatures and chemical species contributing to particle growth at various stages. With PAH nascent to the fuel, the fuel-rich core of a spray would be primed for early soot particle inception by PAH nucleation.[32] PAHs may not be able to stack in a regular manner so as to produce a graphitic structure; the random chaotic assemblage of PAH would lead to a disorganized particle core similar to the one observed here. Moreover, the high chlorine content of the fuel could accelerate radical formation via H-atom abstraction, further accelerating PAH growth, nucleation, and initial particle mass growth at relatively low temperatures.[33] Nearer the flame front, the combination of higher temperatures (1300 °C) and longer times needed to reach this region will foster the breakdown of PAH and fuel

(31) Bond, T. C. Global Black Carbon Estimates (personal communication).

(32) Ragucci, R.; Cavaliere, A.; Ciajolo, A.; D'Anna, A.; D'Allessio, A. Structures of Diesel Sprays in Isobaric Conditions. The Twenty-Fourth Symposium (International) on Combustion, Sydney, Australia, 1992; The Combustion Institute: Pittsburgh, PA, 1992; pp 1565−1571.

(33) Huang, J.; Senkan, S. M. Polycyclic Aromatic Hydrocarbon and Soot Formation in Premixed Flames of CH_3Cl/CH_4 and CH_4. The Twenty-Sixth (International) Symposium on Combustion, Naples, Italy, 1996; The Combustion Institute: Pittsburgh, PA, 1996; pp 2335−2341.
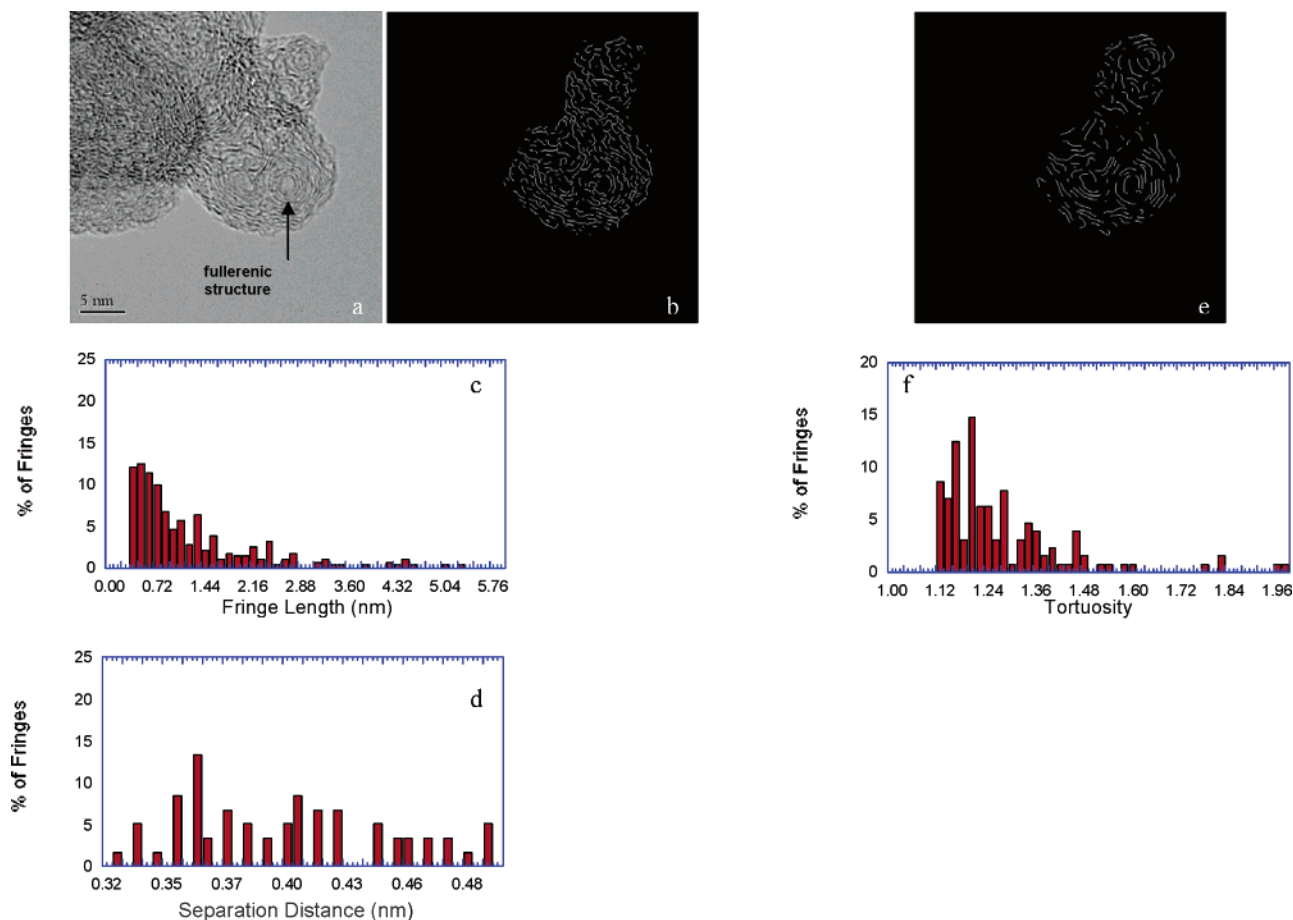
Figure 3. Shown are the bright-field HR-TEM image (a), the corresponding skeleton image (b), derived histograms of fringe length (c) and separation distance (d), the image skeleton for calculation of tortuosity (e), and histogram of fringe tortuosity (f) for the soot derived from the jet aircraft engine exhaust.

components, resulting in acetylene (C_2H_2) formation.[34] C_2H_2 may be able to assemble in an orderly fashion given its size;[33] ordered molecular species addition to the soot particle via the hydrogen addition-carbon abstraction (HACA) mechanism may account for the increasingly ordered structure at these later stages (explaining the particle perimeter).[35] Clearly, the fuel composition and combustion process influence soot nucleation and the subsequent particle growth and chemistry reflected in the nanostructure.

Histograms showing the distributions of lamella fringe length, tortuosity, and separation distance are also given in Figure 1. The fringe-length histogram shows a significant population of fringes with lengths beyond 1.4 nm, an indicator of graphitic structure. The tortuosity is relatively narrowly distributed, signifying that the lamella are not highly curved, consistent with visual inspection of the bright-field image. The range of separation distances is broad, reflecting a turbostratic structure of the lamella.

Operating at just ~40% of its capacity without a particle control device, the smaller institutional-scale boiler (67 GJ) firing distillate oil showed a comparatively lower $PM_{2.5}$ emission factor range of 0.03−0.2 g/kg of fuel burned (for 60 h of testing). However, these emissions comprised considerably more

carbon with as much as 34% being EC on a mass basis (2−34% was the range). Interestingly, the boiler fired with the lighter distillate fuel yields very different soot. As seen qualitatively via the HR-TEM bright-field image and quantitatively by the fringe-length histogram present in Figure 2, the soot nanostructure is relatively disordered with few fringes beyond 1 nm in length. With the smaller design likely possessing better fuel−air premixing and lower temperatures for NO_x reduction, PAHs[36] (nascent or pyrolysis-derived) and oxygenated species likely contribute to particle growth, leading to a less ordered structure.[6] The tortuosity is more broadly distributed than that for the soot produced in the plant-scale boiler, consistent with the more disordered lamella comprising the particle. Because tortuosity reflects undulations of lamella, adjacent lamella are necessarily out-of-registry compared to plane layers so as to minimize $\pi-\pi$ electron repulsions. Correspondingly, the median fringe separation is larger than that for the plant-scale oil boiler soot.

Jet Aircraft Engine Exhaust. Aircraft emissions are a growing concern owing to their affects on climate (cloud condensation nuclei and contrail formation) and potential toxicity. Though generally considered poorly characterized, aircraft particle emissions consistently exhibit a nuclei mode—especially during takeoff (ref 37 and references therein). The cycle-integrated jet engine tests conducted here yielded nuclei

(34) Frenklach, M.; Clary, D. W.; Gardiner, W. C.; Stein, S. E. Effect of Fuel Structure on Pathways to Soot. The Twenty-First Symposium (International) on Combustion, Munich, Germany; The Combustion Institute: Pittsburgh, PA, 1986; pp 1067−1076.

(35) Frenklach, M. On Surface Growth Mechanism of Soot Particles. The Twenty-Sixth (International) Symposium on Combustion, Naples, Italy, 1996; The Combustion Institute: Pittsburgh, PA, 1996; pp 2285−2293.

(36) Benish, T. G.; Lafeur, A. L.; Taghizadeh, K.; Howard, J. B. C_2H_2 and PAH as Soot Growth Reactants in Premixed C_2H_4-Air Flames. The Twenty-Sixth (International) Symposium on Combustion, Naples, Italy, 1996; The Combustion Institute: Pittsburgh, PA, 1996; pp 2319−2326.
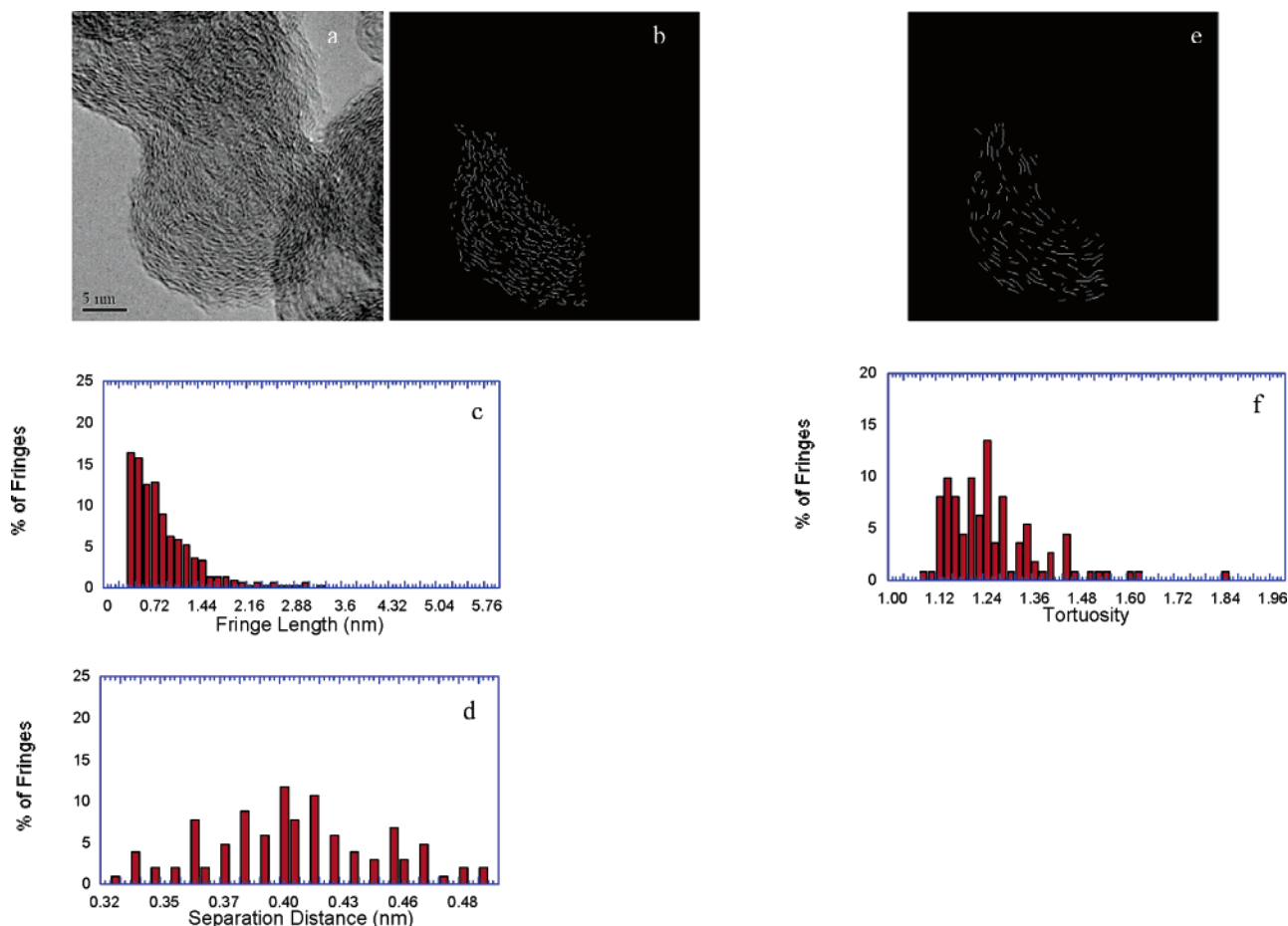
Figure 4. Shown are the bright-field HR-TEM image (a), the corresponding skeleton image (b), derived histograms of fringe length (c) and separation distance (d), the image skeleton for calculation of tortuosity (e), and histogram of fringe tortuosity (f) for the soot derived from the heavy-duty, on-road diesel truck emissions.

mode (<10 nm; number median diameters between 10 and 30 nm) and nanoparticle (<100 nm) emissions, with mass emission factors spanning from 0.02 to 0.2 g/kg of fuel burned. Though higher EC/OC ratios in aircraft PM have been reported,[38] our values ranged between 0.1 and 1 and depended on the fuel composition. These data correspond to an EC emissions span of 0.002 to 0.1 g/kg, which virtually envelops the established range of EC emission factors for jet aircraft engines.[24] Again, jet engine testing rendered limited filter mass of carbonaceous aerosol, precluding organic compound identification through standard analytical chemical techniques (e.g., GC/MS, HPLC). With (i) global EC emissions from aircraft already estimated at 19 Gg/year,[24] (ii) air traffic growth expanding at a rate of nearly 6% per annum,[39] (iii) the proximity of airports to densely populated urban centers, and (iv) the expected increase in atmospheric nanoparticle concentrations due to the implementation of national ambient PM$_{2.5}$ standards, there is an impending need to better approximate and understand this source's soot contribution.

Compared to soot from the oil-fired boilers, the jet engine soot carbon lamella are longer, more parallel, and quite distinct, as shown in the HR-TEM image in Figure 3. There are many regions of localized graphitic structure where several lamella are parallel or similarly curved together. These localized regions extend throughout the particles; their location depending upon the particular image plane. Reflecting some of this graphitic structure, the fringe length histogram, Figure 3, exhibits an extended distribution. Additionally, there are recognizable fullerene-like structures centrally located within the particles (see Figure 3 arrow). Their central location suggests they formed early during the combustion-regulated process of soot generation. Given that the fringes curve about common points, the tortuosity distribution mean is greater than 1 and similar to the plant-scale boiler soot. Similarly, the oriented curvature of adjacent lamella results in the nonregistry of neighboring lamella. As before, given the resulting increased electronic repulsion, increased separation distance is energetically favorable, as marked by the broad, nearly flat fringe separation distribution.

C$_5$-membered rings are an essential ingredient for fullerenic nanostructure; co-integration of C$_5$ into a C$_6$ framework will naturally lead to curvature (fullerenic structure).[40] Fast pyrolysis processes can shift the PAH formation pathway away from one of thermodynamic stability—whereby only C$_6$ ringed structures form—to one where C$_5$ species are preferentially formed.[14] Alternatively, C$_5$ species may be formed from oxygenates undergoing decomposition while within fuel-rich environments.[6,41] Given that JP-8 is sprayed into a combustor operating

(37) Herndon, S. C.; Onasch, T. B.; Frank, B. P.; Marr, L. C.; Jayne, J. T.; Canagaratna, M. R.; Grygas, J.; Lanni, T.; Anderson, B. E.; Worsnop, D.; Miake-Lye, R. C. *Aerosol Sci. Technol.* **2005**, *39*, 799−809.

(38) Hopke, P. K. In *Receptor Modeling in Environmental Chemistry*; John Wiley: Hoboken, NJ, 1985; pp 267−314 (appendix).

(39) International Air Traffic Growth Association. http://www.iata.org (accessed Mar 2006).

(40) Goel, A.; Hebgen, P.; Vander Sande, J. B.; Howard, J. B. *Carbon* **2002**, *40*, 177−182.

(41) McEnally, C. S.; Pfefferle, L. D. *Combust. Flame* **2002**, *129*, 305−323.
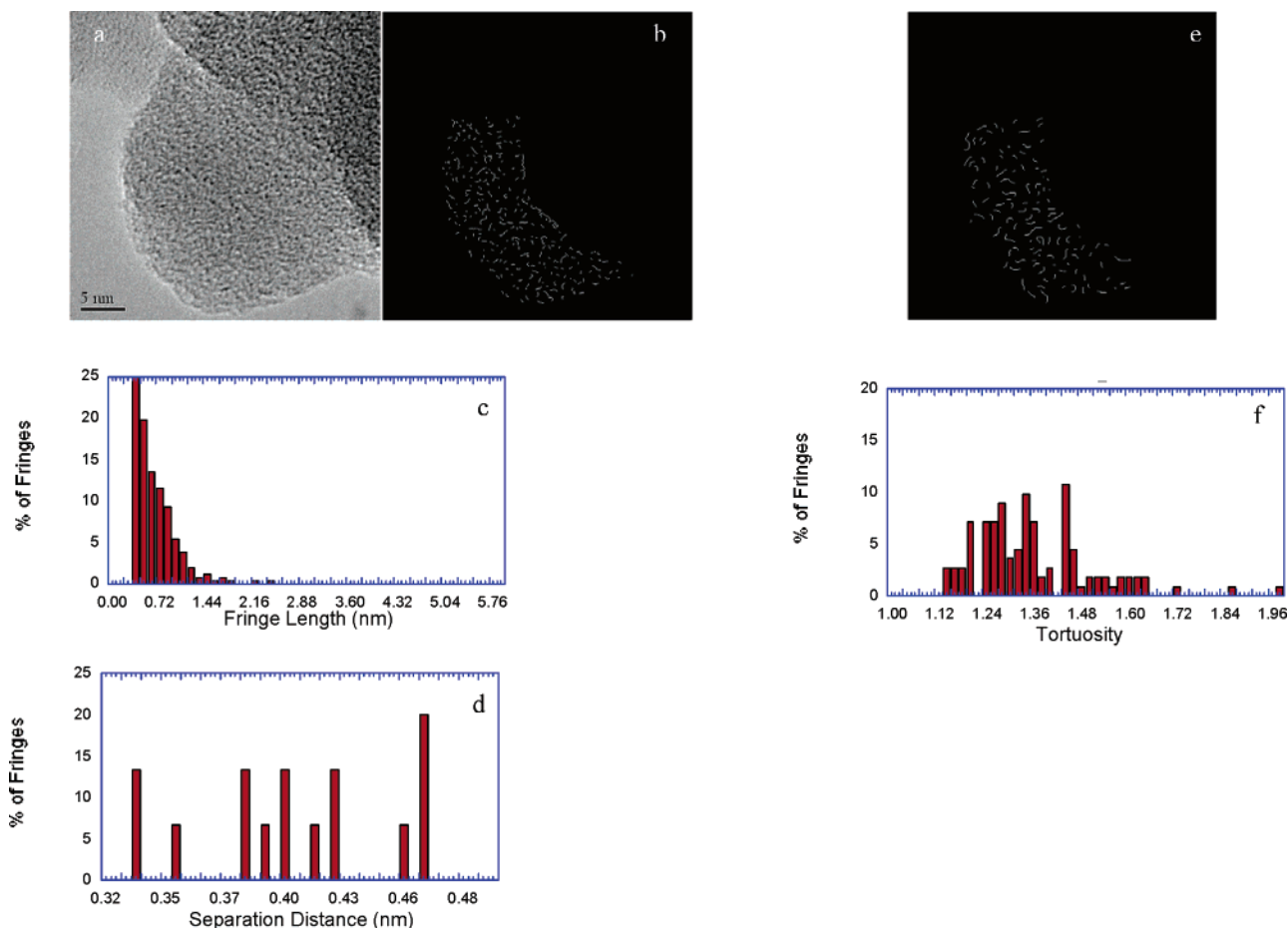
Figure 5. Shown are the bright-field HR-TEM image (a), the corresponding skeleton image (b), derived histograms of fringe length (c) and separation distance (d), the image skeleton for calculation of tortuosity (e), and histogram of fringe tortuosity (f) for the soot derived from the simulated wildfire emissions.

in excess of 2000 °C with very fast fuel−air mixing occurring, both routes for C_5 formation are likely operative. As the sample was integrated over several test cycles including four power settings, further correlation of the nanostructures with engine conditions is not yet possible. However, to the best of our knowledge, this is the first known linkage between fullerene-like molecules and aircraft engine soot.

Utsunomiya and co-workers[42] have identified and tentatively ascribed fullerene cages in atmospheric particle matter to coal combustion soot. Our evidence of fullerene structure in aircraft engine soot demonstrates that fullerene is not unique to a single fossil fuel combustion source. Despite speculation on its presence in wildfire soot,[43] to the best of our knowledge, fullerenic matter has not been directly observed in any type of biomass burning emissions. Perhaps it is reasonable therefore to suggest that fullerenic nanostructure could broadly function as an indicator of fossil fuel combustion emissions in airborne soot particles. Though, we caution that a fullerene deficiency in atmospheric soot would not necessarily be concomitant with a lack of fossil fuel EC in that sample. For one thing, not all coal fly ash soot bears resemblance to fullerene-like structure.[8] Moreover, fullerene contribution from natural sources is a remote possibility. Both of these conditions would disrupt fullerene's potential as a robust indicator of fossil fuel emissions in airborne soot. Nonetheless, supplementary information about

the elemental composition of the source fuel and aerosol, complementary to the nanostructure, can be applied to further resolve the fossil fuel combustion sources contributing to atmospheric soot. In the case of the primary coal combustion particles identified by Utsunomiya et al.,[42] uranium microcrystals were encapsulated in the relatively graphitic carbon bordering the fullerene-like entities. Highly refined JP-8 fuel is not expected to contain uranium, and as expected, we observed no such obvious and refined heterogeneous elements or inclusions in our jet engine sample.

On-Road, Heavy-Duty Diesel Truck Emissions. When considering "contained" combustion, diesel truck emissions are the largest source of EC globally, contributing an estimated 792 Gg/year to the troposphere.[24] Diesel aerosol emissions have been extensively studied and exhibit fractions of EC varying widely (0.2−0.9) as a function of fuel composition, operating conditions, and engine and on-board emissions control technology. The model age (1990) and considerable wear on the long-haul diesel truck engine (>900 000 miles) used in this study likely contributed to the high EC fraction (70% w/w) measured in its PM emissions.

The pervasiveness of diesel emissions has led to the widespread study of diesel soot morphology, though quantitative assessments have been scant (for examples of quantitative measures of soot, see refs 4 and 11). Soot from the diesel engine tested here possesses moderate graphitic structure along the particle perimeter with the interior lamella being more chaotically arranged, as seen in the HR-TEM image of Figure 4, an occurrence somewhat similar to that observed for the plant-

(42) Utsunomiya, S.; Jensen, K. A.; Keeler, G. J.; Ewing, R. C. *Environ. Sci. Technol.* **2002**, *36*, 4943−4947.

(43) Heymann, D.; Chibante, L. P. F.; Brooks, R. R.; Wolbach, W. S.; Smalley, R. E. *Nature* **1994**, *265*, 645−647.

scale oil boiler. Lamella around the particle outer portion are intertwined rather than concentrically stacked. Their rippled arrangement with respect to each other suggests diverse chemical species contributing to nucleation and primary particle growth, both of which can occur in different zones of the combustion flame. It is again speculated that large PAH molecules contributed to nucleation and early growth, forming the particle interiors, while acetylene (C_2H_2) contributed to the latter stage growth at the perimeter. This view was justified in an earlier discussion with the differences here being (i) that the PAHs were likely pyrogenically formed (<1200 °C) in the fuel-rich core of the diesel engine spray instead of being nascent, (ii) the lesser degree to which the perimeter region of the diesel soot contains graphitic structure, and (iii) the relative lack of radial variation in the diesel soot. The clear message is that anthropogenic combustion soots—though refractory and commonly thought of as a single chemically homogeneous entity—are internally mixed carbonaceous assemblages.

By definition, the tortuosity distribution reflects the undulation of the lamella. As seen within the bright-field image, Figure 4, the extent of texturing is prevalent throughout the majority of the particle and particularly along the perimeter. Interestingly, this uniformity gives rise to a modestly peaked separation histogram with very similar mean and median values of ∼0.4 nm.

Ponderosa Pine (*Pinus* sp.) Forest Wildfire. We burned a mixture of dead understory litter and fresh tree canopy (8–33% moisture) biomass typical of that consumed in a western U.S. wildfire. Its resinous nature made this fuel mixture highly flammable, which resulted in a high number (>1 million/cm^3) of accumulation mode (merged primary) particle emissions (unimodal log-normal distribution centered at approximately 200 nm).[26] The emissions factor for EC was 0.4 g/kg, in good agreement with the EC emission factor values compiled in ref 44. Numerous factors potentially affect the fraction of EC in PM from biomass combustion. These include fuel type, moisture content, loading, texture, ecosystem, landscape, soil conditions, fire type, and prevailing meteorology just to name a few. The open burning of biomass is the single largest global source of atmospheric EC emissions—totaling approximately 3.3 Tg/year.[24]

As Figure 5 illustrates, soot from the simulated wildfire emissions is amorphous, in stark contrast to the other soot. The distribution of fringe lengths is narrow and peaks near 0.6 nm with greater than 85% of the fringes being less than 1.0 nm in length. Such short lamella (i) lead to a highly chaotic nanostructure with a wide range of interplanar spacings, (ii) will have a relatively larger fraction of carbon atoms at edge sites, and (iii) do not support significant curvature (hence, less significance should be ascribed to the breadth of the tortuosity distribution relative to a graphitic soot, i.e., soot from the plant-scale boiler). These observations point to substantially different particle nucleation and growth mechanisms occurring in biomass fire plumes. The deficiency of nuclei in the wildfire sample was also observed in a wood stove soot and likely due to particle growth by condensation.[45] The deficiency of fullerene nanostructure in the biomass burning aerosol is noted.

Biofuels such as cellulose, lignite, and so forth tend to create a multitude of pyrolysis products, many of which evolve at moderate temperatures where smoldering rather than flaming combustion occurs.[46] Within amorphous soot nanostructure, hydrocarbons, oxygenates, and hydrogen are more prevalent, and they terminate the edge-site carbon atoms and fill or partially occupy void volumes within the composite particle. Assimilation of these interstitial molecular species or chemical functional groups into the soot structure likely contributes to the disorganization given the inhomogeneity of surface radical sites and the many steric and conformational possibilities. Hydrogen or other chemical species terminating the edge site carbon atoms may also contribute to the lack of planar lamella observed. Notably, the lower thermal stability of these molecular species or chemical functionalities is consistent with the overall formation of the soot particle at lower combustion temperatures.

In summary, numerous individual carbon-bearing particle types have been ascribed to biomass burning.[10] The observed amorphous nature of the soot from the Ponderosa Pine wildfire simulation was also noticed in biomass fire aerosols sampled from several of earth's continents (refs 9 and 10 and references therein). Despite the stark contrast between wildfire soot and other combustion soot, a similar amorphous structure has been attributed to organic carbon matter in biogenic particles.[9] The mass proportion of inorganic elements in the biomass combustion and biogenic particles is likely to differ and perhaps be functional for apportionment. It remains to be seen if the lattice fringe analysis of these analogously structured wildfire and biogenic carbon particles would exhibit any significant statistical differences. The biomass fire aerosol is unique in that a large fraction of organic matter—deficient in other examined soot particles—shields its framework and seemingly interferes with the soot's ability to further organize.

Evidence of Combustion Source Soots in Ambient Samples. Figure 6 images a–d exhibit the wide range of nanostructures observed in the Northern Front Range sample. For example, image a in the figure shows particles that possess a radial variation in nanostructure, as indicated by lamella length and organization. Examples of core–shell arrangements may be viewed in Figure 6 image b. These soot particles possess a disorganized core and outer graphitic structure where the lamella are observed as parallel or similarly curved. Fullerene-like structures (image c) and a largely disorganized nanostructure (image d) are also detected in the particles collected at the Northern Front Range. Clearly, its heterogeneous nature indicates that sources with different combustion processes including fuel, fuel–air ratio, and combustor type contribute to this sample. The results of the lattice fringe analysis as illustrated by the previous samples would be distinct for each type of illustrated nanostructure. Given the observed similarity in nanostructure between these and prior soots, a tentative assignment of the origins of these soots would be (i) power plant or similar large-scale industrial source, (ii) jet aircraft, and (iii) biomass burning sources, respectively.

Of particular interest is the variability of soot nanostructure observed in the Duke Forest tree canopy as shown in Figure 7. Qualitatively, the samples exhibit a range of nanostructures; the different selected images are not meant to convey the relative proportion of each type of nanostructure but rather to illustrate the range observed. Largely distinguishing these soot samples are the observable lengths of the lamella and their local organization (or lack thereof). The radial variation of the nanostructure and outer graphitic structure is consistent with the formation mechanisms previously discussed. Such wide

(44) Andreae, M. O.; Merlet, P. *Global Biogeochem. Cycles* **2001**, *15*, 955–966.

(45) Kocbach, A.; Li, Y.; Yttri, K. E.; Cassee, F. R.; Schwarze, P. E.; Namork, E. *Part. Fibre Toxicol.* **2006**, *3*, DOI: 10.1186/1743-8977-1183-1181.

(46) Molto, J.; Conesa, J. A.; Font, R.; Martin-Gullon, I. *Environ. Sci. Technol.* **2005**, *39*, 5141–5147.
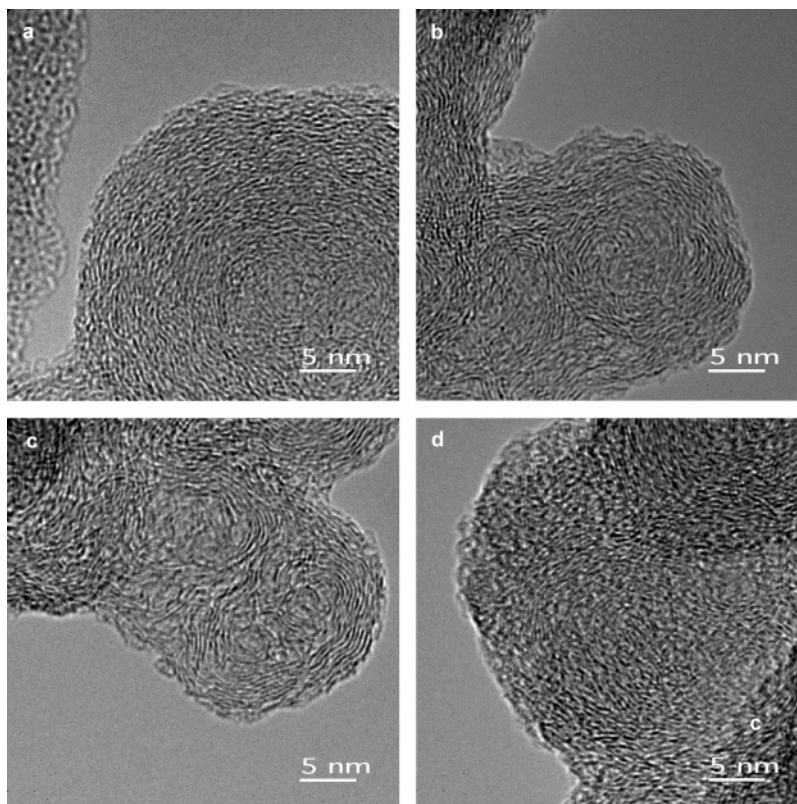
Figure 6. Survey HR-TEM images of soot collected from the Northern Front Range Air Quality Study. Different types of nanostructure readily recognizable by their lamella organization include (i) radial variation of lamella length and organization (image a), (ii) a core−shell arrangement (image b), (iii) fullerenic-like structures (image c), and (iv) a largely disorganized nanostructure (image d).
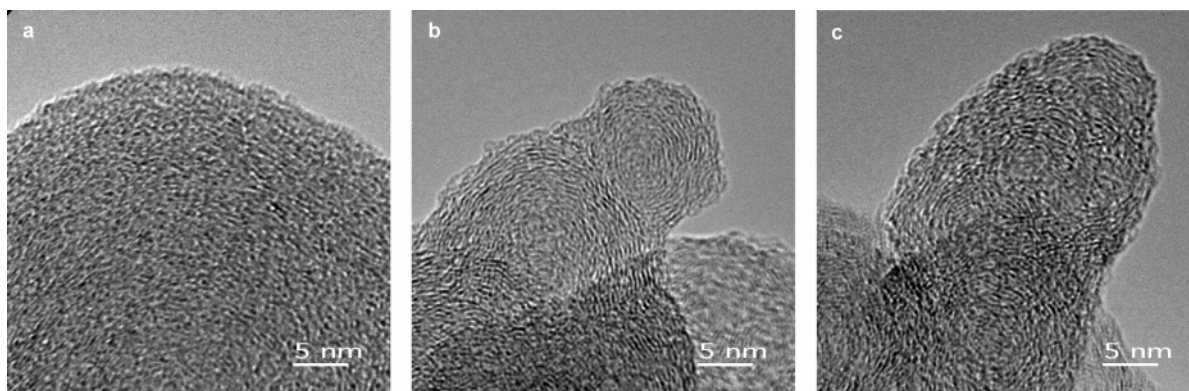
Figure 7. Survey HR-TEM images of soot collected from the ambient PM$_{2.5}$ collected in the Duke Forest. Different types of nanostructure readily recognizable by their lamella organization include (i) amorphous (image a), (ii) core−shell structure (image b), and (iii) homogeneous structure (image c).

differences in nanostructure within ambient soot suggest that sources with quite different combustion conditions have contributed to the collected sample.

Figure 7 image a shows a nearly amorphous nanostructure. This is likely due to the biogenic contribution to the aerosol. Carbon isotope analysis suggests a relatively large proportion of this mass was biogenic in nature. The amorphous nanostructure could also originate through the combustion of wood or other cellulosic materials of biogenic origin including home fireplaces, wood stoves, and so forth. However, potassium data and meteorology do not support a significant fire contribution, as mentioned. A core−shell structure where the shell consists of parallel lamella about a core of disorganized material is shown in Figure 7 image b, whereas image c exhibits a rather homogeneous structure. Comparatively, the core−shell nanostructure suggests an anthropogenic origin. The marked variation between the particle core and shell, coupled with the recogniz-

able lamella length and stacking in the particle perimeter, suggests origins from sources with markedly different conditions for particle nucleation versus growth, such as a power plant or other similar large-scale facility. Finally, the shorter, more tortuous lamella observed in image c suggest rapid formation, while the lack of radial variation suggests common conditions for particle inception and growth as perhaps may occur in a diesel engine. This result likely confirms the presence of vehicle soot from a local access road and possibly from the thickly settled region surrounding the forest.

Identification of source-specific soot nanostructure in ambient PM samples is apt to be complementary to ongoing source-receptor studies. A positively identified source soot entity in ambient PM presumably could confirm source profile selection prior to developing a chemical mass balance model or could confirm the results (the number and assignment of source types contributing to an airborne aerosol sample) of a positive matrix

factorization. The positive identification of soot nanostructure in source aerosols that are devoid of source-specific or, for that matter, any organic markers is also expected to improve our ability to properly account for the sources contributing to the carbon fraction in ambient PM.

Conclusions

The nanoheterogeneity among soot from different anthropogenic combustion sources was made evident. Important differences in the type and concentration of hydrocarbon assemblages between the particle perimeter and central core were observed across the examined combustion systems. The morphology and nanostructure of biomass burning aerosol stood in stark visual contrast with fossil fuel combustion soot, whereas lattice fringe analysis was needed to reveal the relatively subtle differences among the fossil fuel soot samples. HR-TEM analysis indicated

a wide assortment of combustion sources contributing to atmospheric soot. As it stands now, the determination of source soot nanostructure is likely to complement the development of widely used air-quality models. Further development of apportionment models and the mechanisms underlying the adverse health effects of aerosols are likely to benefit from a better understanding of soot nanostructure.